Chapter 3

Soft magnetism in nitrided $Fe_{93}Ni_4Cr_3$ and $Fe_{94}Ni_4Ti_2$ cold rolled alloys

We investigate the possibility to create an ultrasoft magnetic material by phase transformations after a reduction process of **$Fe_{93}Ni_4Cr_3$** and **$Fe_{94}Ni_4Ti_2$** alloys. The initial idea was that a nanocrystalline structure of a different magnetic phase (γ') can be induced by nitriding. CrN or TiN precipitates formed in a preliminary step were considered nucleation centers for the new phase. This did not work since the precipitates were coherent with the matrix. The second route to refine the crystalline structure was cycling through ε -phase. Although grain refinement is observed after cycling and an almost random orientation of the grains is obtained, the magnetic properties do not improve. This is due to the fact the grain size is still too large to lead to averaging out of the magnetic anisotropy. Moreover, the stress/strain distribution developed during the treatments hampers domain wall motion and leads to an increased coercivity. Since these two ideas did not have a positive output, the study was turned towards understanding the influence of phase transformations on magnetic properties of our alloys considering all aspects related to structure (different magnetic phases, texture, grain size, nitrogen concentration, stress/strain). This systematic study allows as obtaining materials with coercive fields H_C as low as 0.5Oe (samples containing TiN precipitates). For the Cr containing samples, a concentration of 14% $(Fe\text{-}Ni)_4N$ (γ') phase decreases H_C below values corresponding to the samples containing only CrN precipitates.

3.1. Introduction

It is well known that small grains combined with a random orientation can result in very soft magnetic properties, with coercive force below 1Oe [1,2]. Such a behavior is due to a reduction of the effect of the intrinsic magnetocrystalline anisotropy when the average grain size is smaller than the ferromagnetic exchange length (about 35 nm for Fe). Materials that satisfy these requirements are usually obtained by crystallization from the amorphous state. In principle, polycrystalline rolled foils could form an interesting alternative because it would be cheap and applicable to a large thickness range. Small grains could be obtained by direct and reverse phase transformations.

Due to their high saturation magnetization and thermal stability, a promising system is cold-rolled Fe-M-N, where M stands for a few percent of metal with a high affinity for N like Cr, Ti, Zr, Al etc. The reason for choosing an alloying element is that in low-temperature nitriding treatments, small MN precipitates are formed and may influence the formation of an iron nitride phase in a subsequent treatment. This has been demonstrated in recent publications of our group [3-5].

An important issue, which has to be addressed in order to obtain an ultrasoft magnetic material via phase transformations, is the initial texture, which is formed after rolling. Depending on the characteristics of the formation of MN precipitates and subsequent growth of one or more Fe-nitride phases, this initial texture may hamper the formation of randomly oriented grains.

The aim of this chapter is to present the effect of low-temperature nitriding treatments on the magnetic properties of $Fe_{93}Ni_4Cr_3$ and $Fe_{94}Ni_4Ti_2$ cold rolled alloys. We show the optimum conditions for obtaining a soft magnetic material and also what are the consequences of subsequent phase transformations from the point of view of magnetic and structural properties.

3.2. Magnetic (Fe-M) nitrides – structure and magnetic properties

In this section we give a succinct description of the significant magnetic iron nitrides which are subject of the present study. The influence of an alloying element is also discussed.

When quenched from the γ-Fe-N phase, a mixture of bcc and bct phases is formed. The newly tetragonal distorted bct matrix is obtained as a result of accommodation of the nitrogen atoms in the octahedral interstitial positions [6]. This phase is called α' and has a metastable character at room temperature because the

equilibrium solubility of nitrogen in the pure bcc iron lattice is only 0.4 at %. The maximum concentration of nitrogen in α' is 12.5 at%.

If we introduce a substitutional element in the bcc lattice, the nitrogen concentration can increase significantly above the solubility limit in pure Fe, depending on the nitriding conditions, the type and concentration of the alloying element [7]. In the XRD data an asymmetry of the line-shape together with a shift towards lower angles is observed, which is the result of an overall dilation of the lattice.

The saturation magnetization of a (Fe-M-N) alloy containing less than 3 at % of M and only α' phase, is very close to the value of nitrogen-free samples. For nanocrystalline films, thermo-magnetic treatments can lead to a well-defined uniaxial anisotropy due to a preferred occupation of the nitrogen atoms in planes perpendicular to the applied magnetic field [8]. The N atoms will be placed in the octahedral interstitial positions along the most favorable <100> rows breaking the cubic symmetry and creating a magnetic anisotropy parallel to the orientation of the magnetization during the treatment.

The Fe_4N or γ' phase has a fcc unit cell with the nitrogen atom placed in the center of the cube. When extra elements like Mn or Ni are added, these atoms will prefer to occupy the 1a sites at the corners of the unit cell [9, 10]. At room temperature the saturation magnetization of γ' is 1.9 T. Ferromagnetic resonance measurements on sputtered single-crystal $(Fe\text{-}Ta)_4N$ films give a value of the cubic anisotropy constant $K_1 = -1.5 \times 10^4$ J/m^3[11].

Another magnetic iron nitride is $Fe_{3-x}N$ or ε with a hexagonal structure. The compound is ferromagnetic with a saturation magnetization much smaller than that for bcc iron. With increasing x, the Curie temperature decreases. At room temperature, the ε phase is nonmagnetic for $x > 0.67$ [12].

3.3. Experimental

Foils of 2 to 6 μm thick were produced by cold-rolling of 0.5 mm $Fe_{93}Ni_4Cr_3$ or $Fe_{94}Ni_4Ti_2$ bulk alloys. By admixing Ni we have increased the plasticity of the materials. Nitridings were performed in a circulating gas mixture of $NH_3 + H_2$ at temperatures between 300 and 500°C for time intervals from 1 to 34 h, depending on the estimated kinetics of nitridation. An important parameter is the nitriding potential $R_N = \ln[p(NH_3)/p(H_2)^{3/2}]$, where the pressures of ammonia, $p(NH_3)$, and of hydrogen, $p(H_2)$, are in Pa. The plot of R_N versus T, called the Lehrer diagram, shows the stability of the various Fe-nitride phases in the presence of a NH_3/H_2 gas mixture [13, 14]. In Fig. 3.1 we present this diagram together with the coordinates of the points corresponding to the nitriding experiments presented in this chapter.

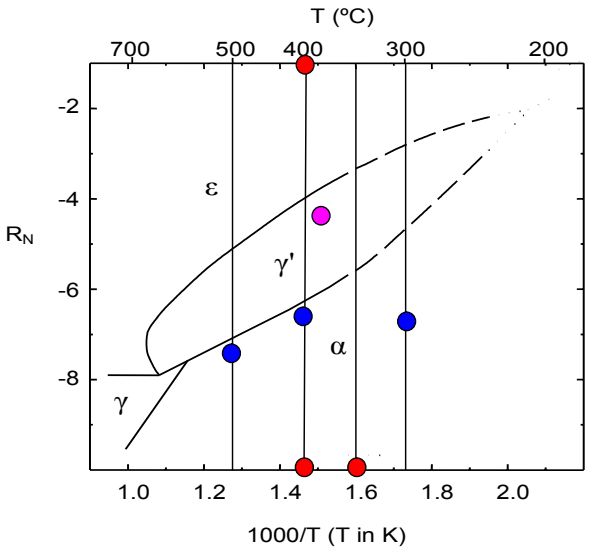

Fig.3.1. The nitriding parameters in the Lehrer diagram [13].

As standard tools for structural investigations, we have used conventional Transmission Mössbauer Spectroscopy (MS), X-Ray Diffraction (XRD) and Transmission Electron Microscopy (TEM). It is important to mention that the use of Mössbauer Spectroscopy allowed quantitative estimations concerning the precipitates formation and used also to determine the relative amount of the various phases. In order to determine the nitrogen concentration, the samples were weighted before and after the treatments. The magnetic characterization was performed with a Vibrating Sample Magnetometer (VSM) and a Superconducting Quantum Interference Device (SQUID) magnetometer.

3.3.1. Results and discussion

The applied thermochemical treatments in our experiments are summarized in Table 3.1.

3.3.1.1. Nitriding in the α region.

For as-rolled materials a strong texture dominated by the (002) reflection was observed in θ-2θ XRD patterns. There is also an appreciable texture in the surface plane, the rolling direction being a <110> axis. In addition an appreciable fraction of

Table 3.1. Nitriding conditions

α' $(Fe_{94}Ni_4Ti_2)_xN_{1-x}$

Sample Name	Treatment
T1	As rolled
T2	Annealed 300°C / H_2 atm. / 21h
T3	Nitrided 300°C / $\ln(R_N)$ = -5.08 / 21h
T4	Nitrided 300°C / $\ln(R_N)$ = -5.08 / 21h followed by annealing at 600°C / H_2 atm. / 16h
T5	Annealed 400°C / H_2 atm. / 21h
T6	Nitrided 400°C / $\ln(R_N)$ = -6.78 / 4h
T7	Nitrided 500°C / $\ln(R_N)$ = -7.3 / 1h

$\alpha' \rightarrow \gamma'$ $(Fe_{93}Ni_4Cr_3)_xN_{1-x}$

Sample name	Treatment
C1	As rolled
C2	Nitrided 500°C / $\ln(R_N)$ = -7.34 / 1h
C3	Nitrided 500°C / ln (R_N) = -7.34 / 1h followed by nitriding at 380°C / $\ln(R_N)$ = -4.68 / 4h
C4	Nitrided 500°C / ln (R_N) = -7.34 / 1h followed by nitriding at 380°C / $\ln(R_N)$ = -4.68 / 10h
C5	Nitrided 500°C / ln (R_N) = -7.34 / 1h followed by nitriding at 380°C / $\ln(R_N)$ = -4.68 / 22h
C6	Nitrided 500°C / ln (R_N) = -7.34 / 1h followed by nitriding at 380°C / $\ln(R_N)$ = -4.68 / 34h

Cycling $(Fe_{93}Ni_4Cr_3)_xN_{1-x}$

Sample name	Treatment	Nr. of cycles
C7	α→/400°C/→ε→/400°C /→α	1
C8	α→/400°C/→ε→/400°C /→α	5
C9	α→/400°C/→ε→/400°C /→α	12
C10	α→/400°C/→ε→/300°C /→α	1
C11	α→/400°C/→ε→/300°C /→α	2
C12	α→/400°C/→ε→/300°C /→α	5
C13	α→/400°C/→ε→/300°C /→α	6

grains was found with a <222> axis perpendicular to the surface. This fraction shows much less anisotropy in the plane of the sample. TEM measurements revealed a strongly defected microstructure. We have observed grains presenting a slip plane system with the distance between the slip planes about 100-300 nm, in agreement with previous measurements [15]. Complementary Scanning Electron Microscopy showed crystallites with an in-plane size on the order of microns, but not more than 25 μm, and a thickness on the order of hundreds of nanometers.

After the nitriding treatments in the α region a homogenous precipitation of fcc CrN or TiN was observed. In both cases, the Bain orientation relationship [16, 17] with respect to the bcc matrix was observed, i.e. $(100)_{fcc}//(100)_{bcc}$ and $[01\bar{1}]_{fcc}//[001]_{bcc}$. For the Ti alloy, formation of nanometer thin TiN platelets was identified already after nitriding at 300°C. This is accompanied by an appreciable nitrogen uptake, 2 at% in the TiN precipitates, plus about 3 at% in the form of interstitial nitrogen. At 400°C, CrN precipitates grow as platelets with a thickness of about 1 nm. Even after 24 h the precipitate process is not completed. Another type of CrN precipitates is formed after nitriding above 500°C. These are bigger and not coherent with the matrix. Still many coherent precipitates are present even after nitriding at 600°C, as evidenced by intense streaking of {200} spots of TEM diffraction patterns (DP) [4].

In the following part we will discuss the results of the magnetic characterization for the samples nitrided in the α region. The results are given in Table 3.2. Most of the measurements have been done in two directions, parallel and at 45° with respect to the rolling direction. We can see in Fig. 3.2. that the approach to saturation is similar in both as-rolled and α -nitrided samples. The anisotropy reflects the in-plane texture. In the 45° case, the field is predominantly oriented along a <100> easy axis

Table 3.2. DC magnetization parameters in α nitrided Ti- contained samples

Sample name	Interstitial Nitrogen at%	H_c (Oe)	μ_i
T1	-	5.5	606
T2*	-	4.5	940
T3**	3	2	820
T4**	0.5	1	810
T5*	-	3	1100
T6**	1.5	0.5	1200
T7**	2	3	890

μ_i = initial permeability calculated in the region where the hysteresis loops measured in both directions are superposed.
*) annealed samples.
**) nitrided samples.

for the grains with a <001> surface normal. The remaining tail is due to the fact that i) the planar texture is not complete for these <001> grains and ii) the <111> oriented fraction has no significant texture in the surface plane.

Nitriding in the α region does not change this planar texture. However, the coercive force H_C decreases by an order of magnitude for both directions of the external magnetic field. In principle various factors can contribute to this effect. As already mentioned, nitriding leads to i) precipitate formation, ii) lattice expansion and associated uptake of interstitial nitrogen (especially for the Ti-alloy) and iii) partial annealing of defect structures.

To make a clear distinction between the influence of the defects and of nitrogen, we have annealed the (Fe-Ti-Ni) samples in a H_2 atmosphere at the same temperatures as used for nitriding. The results show that both effects play a role, but the lattice expansion/ presence of interstitial N is the dominant factor in the reduction of H_C (compare T2/T3 and T5/T6 in the Table 3.2.). Here, the interstitial nitrogen is obtained by subtracting the quantity associated to precipitates from the concentration calculated by weighing.

The effect of annealing is easy to understand: removal of defects decreases the number of pinning centers for the domain walls. The influence of interstitial nitrogen may have to do with the change in magnetostrictive properties. It is known [18] that for pure iron the magnetostriction constant depends linearly on the nitrogen content

with a zero crossing at about one atomic percent nitrogen. Because our samples have a different microstructure and a different composition, the zero crossing may take place at another N concentration. Moreover, it may be different for the Cr-alloy and the Ti-alloy. A significant decrease of the magnetoelastic constant renders the domain structure much less sensitive to local stresses. This will lead to a simple domain structure with larger domains and will decrease H_C accordingly.

For any in-plane orientation of the DC field, we have measured values for the remanent magnetization M_R below 50% of the saturation magnetization. A systematic decrease of M_R as a function of increasing N content was observed in both alloys. For the samples where we expect to have the lowest values of magnetostriction we found

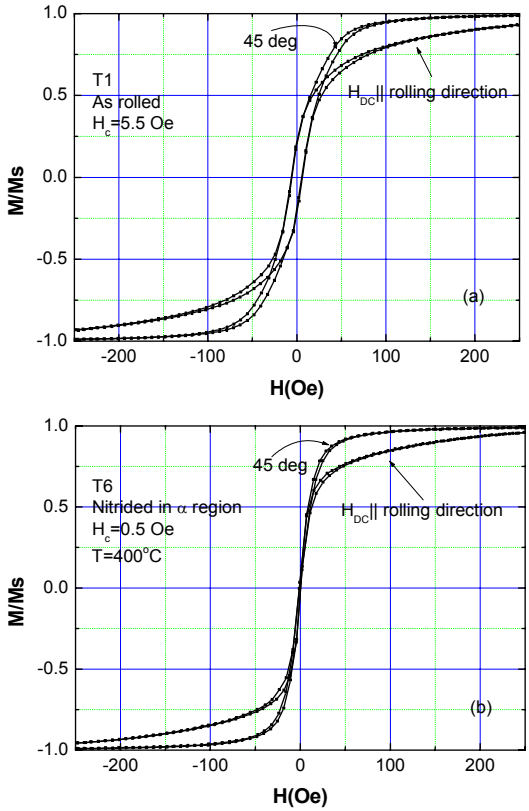

Fig. 3.2. DC hysteresis loops for (Fe-Ni-Ti) alloy: a) as rolled and b) nitrided at 400°C / R_N = -6.78 / 4h.

the lowest values of M_R, see Fig. 3.2(b). If we consider the magnetoelastic coupling between the grains as the possible origin of this effect, then we would expect an opposite behavior [19]. This statement is based on the experimental observation that in the case of soft polycrystalline ferrites, when the magnetostriction constant becomes negligibly small, the remanent magnetization increases close to the M_S value. Another important factor which in principle can influence the remanence is the grain orientation. For a random orientation of the crystallites, the value of M_R is 0.8 M_S, assuming a cubic anisotropy. Even more, there is no preferential grain orientation that can lead to a remanence value below half of the saturation magnetization.

We conclude that in our materials the magnetostriction has an indirect contribution in lowering the remanent magnetization by decreasing H_C. The low M_R has to do with the thickness of the foils (6 μm). The aspect ratio determines an in-plane demagnetizing field $H_D=NM_S$ of around 15 Oe [20], where N is the demagnetizing factor. In order to minimize the sum of magnetostatic and Zeeman energy the domain pattern in the sample will try to adjust such that $NM=B_{ext}$, implying that $\mu = \frac{1}{N} \cong 1400$. This agrees reasonably well with the measured value (see Table 3.2), indicating that the domain walls can move easily.

Using transmission Mössbauer spectroscopy we have estimated the average angle θ of the magnetization with respect to the plane of the sample [21]; these measurements were done at the remanence. The calculated θ was between 10 and 30°, leading to the conclusion that the magnetic domain pattern must contain closure domains in order to keep a minimum value of the total energy of the system.

3.3.1.2. Nitriding in the γ' region

To study the formation of the γ' phase in samples containing precipitates formed at 500°C, we performed nitriding at 380°C for different time intervals, see Table 3.2. The speed of the α→γ' transformation depends on the nitrogen uptake rate and is almost linear versus time. In Fig. 3.3. we present the XRD θ-2θ scans of sample C2, nitrided in the α region and containing CrN precipitates, and C6, a sample containing 95% γ' phase. We can see that the γ' phase develops a texture having mainly the planes $(200)_{\gamma'}$, $(220)_{\gamma'}$ and $(420)_{\gamma'}$ parallel to the surface. This is in agreement with the Bain relationship mentioned earlier.

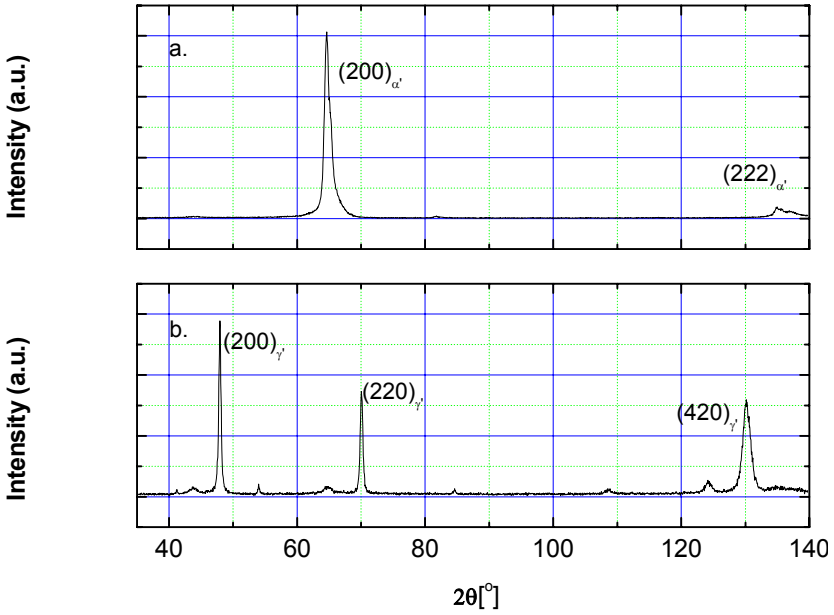

Fig. 3.3 XRD patterns for a) sample C2 and b) sample C6.

Each reflection in the XRD spectra of the γ' phase corresponds to a set of crystallites which were transformed from the α phase. The γ' crystallites with the planes (200) and (220) parallel to the surface can be considered as a result of the transformation of (200) α- crystallites and the γ'-crystallites with (420) plane parallel to the surface correspond to (222) α-crystallites. This is obtained roughly by a rotation of the initial α cell by 45° in the (100) plane.

The widths of the γ' peaks in the XRD patterns have the same value in the full range of concentration. This implies that during the growth of the new phase the combined effect of microstrain and grain size remains constant. The evolution of CrN precipitates during γ' nitriding is illustrated in the Figs. 3.4 and 3.5. For the sample containing 14% γ'- phase, we have observed {200} streaking in the TEM diffraction pattern (DP), as shown in Fig. 3.4. This indicates that the precipitates in the remaining α phase are still 2D platelets. When the amount of γ' phase increases up to 95 %, the streaking vanishes (Fig. 3.5 (c)). Instead, 3D particles of about 30 nm are observed in dark field and bright field images (BF), as shown Fig. 3.5(a) and (b). In accordance with XRD results, γ' grains have a variety of orientations and the grain size is reduced to 200 – 500 nm, as illustrated in Fig. 3.5. Note that the bright area in Fig. 3.5 (a) is in fact a group of many grains of both γ' and α phases producing the most intense diffraction spots (Fig. 3.5(c)), selected for dark field imaging.

The magnetization curves of (Fe-Ni-Cr)-N alloys at various stages of nitriding are shown in Fig. 3.6. A reduction of the coercive force is observed for the

samples containing less than 20% γ'. Above this concentration H_C increases fast up to 45 Oe for a sample consisting of 95% γ'. The same value was observed in single-crystal-like Fe_4N [22], suggesting that this value is related with an intrinsic property of this phase. In the two-phase region, the behavior of the magnetization is affected by a combination of intrinsic properties of the two phases, like magnetocrystalline anisotropy and magnetostriction, and microstructural parameters like crystallite size and texture. In the following we will discuss how these factors can induce changes in the magnetic behavior of the samples.

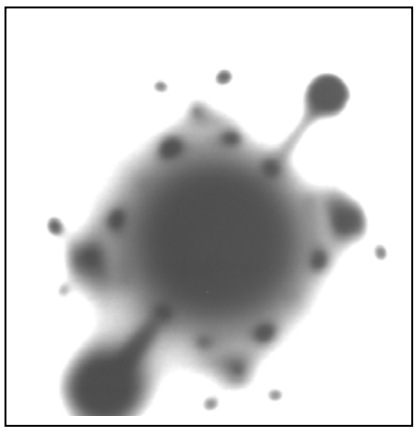

Fig. 3.4. Streaking effect for {200} spots in TEM diffraction pattern of sample C3.

At low concentrations of γ' the host α crystallites will have the dominant effect on the macroscopic magnetic properties. This explains why the shapes of the hysteresis loops are similar for sample C2 and C3. The smaller coercivity of sample C3, having 14% γ', can be a result of two different factors: the magnetostriction of the

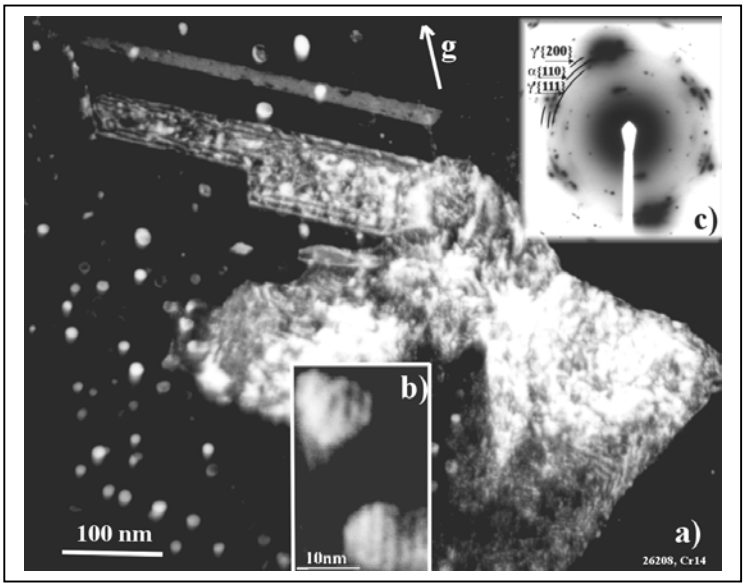

Fig. 3.5 a) A DF image is shown for sample C6, containing 95%γ' phase and b) enlarged image of small particles -CrN precipitates. Compared to the as-rolled foil, the grain size is reduced to 200-500 nm. c) The DP shows a combined contribution of a number of grains of γ' and α-phases.

α phase and the magnetic anisotropy of the γ' crystallites. Due to the strain fields created at the interface between the phases a local bcc lattice expansion is expected. As a consequence more nitrogen is absorbed in the α phase and the value of the magnetostriction constant can be closer to zero. However the interface region can be significant only for γ' crystallites on the order of ten nanometers, which makes this explanation less probable. The second possible explanation is that when averaging over the entire sample containing two phases with anisotropy constants having opposite signs, the total free energy is lowered. We mention that a similar decrease of H_C with the onset of γ' phase formation was obtained by Hoshi and Naoe [23]. The samples studied by them were thin Fe-N films with a $(110)_{\alpha'}$ texture. However, no quantitative estimations of the phases were presented so it is difficult to have a direct comparison with our samples.

For the samples having a γ' concentration higher than 20% the linear increase of H_C is mainly because the magnetic contribution of the new phase to the total energy of the system becomes more significant than that of the α phase.

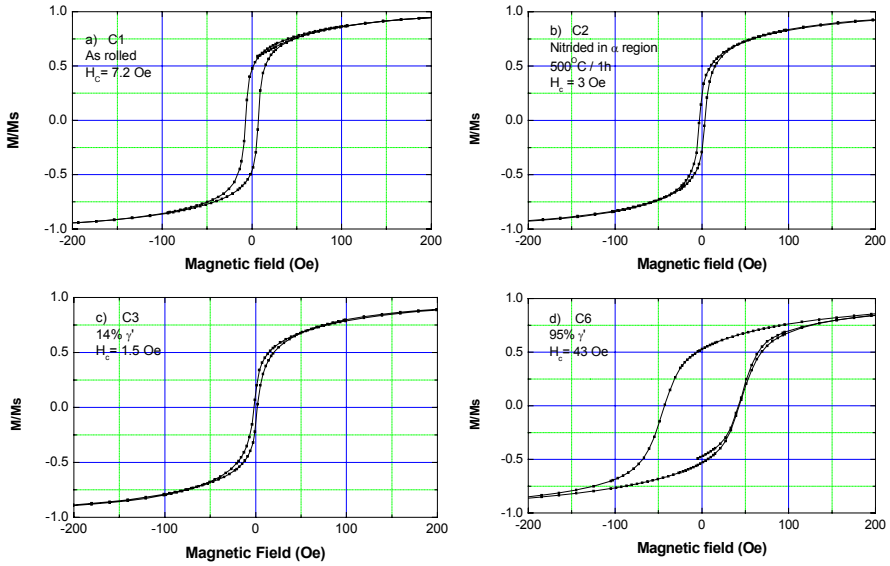

Fig. 3.6 Selected DC hysteresis loops of (Fe-Cr-Ni)–N samples: measurements with the field parallel to the rolling direction.

All samples containing γ' grains present tails in the hysteresis loops, see Fig. 3.6. The magnetic anisotropy is not averaged out because i) the grains are still larger than the ferromagnetic exchange length, and ii) the texture prevents an effective averaging anyway.

3.3.1.3. Cycling

We call cycling the nitriding treatment in which the sample is transformed into a complete iron nitride phase and subsequently reduced in pure H_2 to reform the α phase.

In principle, this procedure may lead to grain refinement and reduction of the initial texture. Indeed, depending on the intermediate phase during the cycling process and on the number of cycles, it is possible to reduce the initial texture. This has been shown in detail elsewhere [5]. While the fine CrN precipitates may lead to a reduction of the initial texture, the presence of the TiN precipitates has an opposite effect. The

TiN precipitates act as phase stabilizers and lower the speed of the intermediate transformation. The removal of the defects induced after rolling may also slow down the process by increasing the kinetic barrier of the transformation. It is required that the cycling is carried out at low temperatures so that the grain growth is suppressed, but at the same time the temperature has to be high enough in order to have a reasonable speed of nitriding. We have chosen the ε as intermediate phase and for the reasons mentioned above, the temperature of nitriding was 400°C. No nitriding in the α region was performed before these experiments.

In Table 3.3 we present the texture evolution of the Cr-alloy. The area ratios A_{200}/A_{110} and A_{211}/A_{110} of (200) / (110) and (211) / (110) XRD lines are to be compared with the values for a random oriented material, which are 0.13 and 0.22, respectively. An almost complete disappearance of the texture is obtained after 12 cycles. Extra information on the structural characteristics was obtained by TEM measurements, see for example Fig. 3.7 (a) and (b). Besides the most pronounced [311]-pole grains, a number of smaller grains with different orientation contribute to the diffraction pattern (Fig. 3.7 (a)). The splitting and the arc-shape reflections are due to the presence of distinct α + α' regions with different N concentration, formed during the reduction treatment. In Fig. 3.7 (b), the contribution to the bright area in the DF image is from a collection of many grains with a size of 100 – 200 nm.

After the first cycle, a sudden increase of the coercive force is observed, followed by values which are all still bigger than the H_C value of the as rolled sample, (see Table 3.3). This behavior can be understood by the evolution of the microstress and texture. The first cycle increases the microstress present after the rolling procedure. This is clearly observed in the XRD measurements: the width of the (200) reflection doubles after the first cycle and then stays constant for the next cycles. The grain size of the samples C7 and C10 was not reduced significantly as compared with that of C1. In this case, the influence of the grain size on the XRD linewidth is only minor.

The relatively large values of the coercivity are associated with the obstruction of the magnetic domain wall movement. Pinning of the domain walls will preferentially occur at grain boundaries between crystallites with a large difference in orientation. An additional contribution to the domain wall pinning is due to the microstress via the magnetoelastic interaction.

Table 3.3. Texture and coercive force evolution in cycled (Fe-Ni-Cr)-N alloy

Sample	Nr. of cycles	Temperature of reduction (°C)	Time of reduction*	A_{200}/A_{110}	A_{211}/A_{110}	H_C (Oe)
C1	-	-	-	-	-	7.2
C7	1	400	2h	3.9	0.7	17.5
C8	5	400	3h10’	0.9	0.3	14.5
C9	12	400	7h	0.2	0.21	42
C10	1	350	3h30’	11	0.7	25
C11	2	350	2h45’	8	0.6	27
C12	5	350	15h40’	1.6	0.3	21.5
C13	6	350	16h	1	0.2	22.5

*) The time of reduction presented here corresponds to the last cycle.

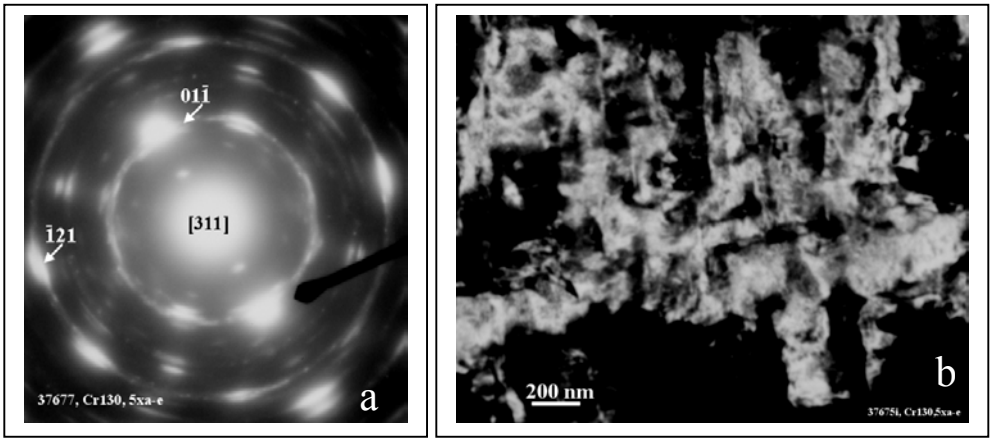

Fig. 3.7.a) TEM DP for the sample C12 and b) the DF image of the same sample.

3.4. Conclusions

The magnetic properties correlated with the structure of (FeNiCr)-N and (FeNiTi)-N alloys were studied. A soft magnetic material was obtained via nitridations in the α' and γ' region of the Lehrer diagram. Our results show that a control of the magnetic anisotropy assisted by the precipitates can be achieved via nitrogen incorporation. The combination of α and γ' phases can improve the soft magnetic properties of the samples. A further investigation in samples with a low concentration of γ' has to be conducted to clarify the origin of this behavior. For this purpose, ferromagnetic resonance measurements can give direct information about the anisotropy fields in the various phases.

Cycling between the α and ε phases leads to a grain refinement in the range of 100-200 nm and the crystalline texture becomes very close to random. However the grain size is still too large to average out the magnetic anisotropy. The microstress distribution is another factor that increases the coercivity in the cycled samples. These last two reasons limit the improvement of soft magnetic properties via the route of grain refinement by solid state phase transformations.

References

1. G. Herzer, IEEE Trans. on Magn. **26**, 1397 (1990).
2. J. Arcas, A. Hernando, J.M. Barandiaran, C. Parados, M. Vasquez, P. Marin and A. Nruweiler, Phys. Rev. B **58**, 5193 (1998).
3. N. G. Chechenin, P. M. Bronsveld, A. R. Chezan, C. B. Craus, D. O. Boerma, J. Th. M. de Hosson and L. Niesen, Mat. Res. Soc. Symp. Proc. **652**, y8.1 (2001).
4. N. G. Chechenin, A. R. Chezan, C. B. Craus, D. O. Boerma, P. M. Bronsveld, J. Th. De Hosson, and L. Niesen, Metal. Mater. Transact. A **33A** (2002).
5. A. R. Chezan, C. B. Craus, N. G. Chechenin, T. Vystavel, L. Niesen, P. M. Bronsveld, J. Th.M De Hosson and D. O. Boerma, submitted to Mater. Sci. Eng.A (2003).
6. P. Ferguson and K. H. Jack, Philosophical Magazine A **52**, 509 (1985).
7. M. Kopcewicz, J. Jagielski, G. Gawilk and A. Grabias, J. Appl. Phys. **78**, 1312 (1995).
8. E. van de Riet, W Klaassens and F Roozeboom, J. Appl. Phys. **81** , 806 (1997).
9. X. G. Diao, A. Y. Takeuchi, F. Garcia, and R. B. Scorzelli, J. Appl. Phys. **85**, 4487 (1999).
10. P. Mohn, K. Schwarz, S. Matar and G. Demazeau, Phys. Rev. B **45**, 4000 (1992).
11. L. Varga and W. D. Doyle, J. Appl. **79** , 4995 (1996).
12. N. DeCristofaro and R Kplow. Metall TransA. **8**, 425 (1977).
13. E. H. du Marchie van Voorthuysen, B. Feddes, N. G. Chechenin, D. K. Inia, A. M. Vredenberg and D.O. Boerma, Phys. Stat. Sol. (a) **177**, 127 (2000).
14. E. Lehrer, Z. Electrochemie **30**, 383 (1930).
15. N.G. Chechenin, A. van Veen, R. Escobar Galindo, H. Schut, A.R. Chezan, P.M. Bronsveld and D.O. Boerma, J. Phys: Condens. Matter. **13**, 5937 (2001).
16. T. Lyman, Metals Handbook: Metallography, structures and phase diagrams, Vol 8 (Am. Soc. Metals Park, Ohio 1973).
17. W. Pitch, Arch. Eisenhüttenw. **32**, 493 (1961).
18. B. Viala, M. K. Minor and J. A. Barnard, J. Appl. Phys. **80**, 3941 (1996).
19. A. Hubert and R. Schäfer, Magnetic Domains, Springer-Verlag, (1998).
20. S. Chikazumi, Physics of Ferromagnetism, Oxford university Press, (1997).
21. U. Gonser, Mössbauer Spectroscopy, Springer-Verlag, (1975).
22. D. M. Borsa, S. Grachev and D. O. Boerma, Appl. Phys. Lett. **79**, 994 (2001).

23. Y. Hoshi and M. Naoe, J. Appl. Phys **69**, 5622 (1991).